



HAL
open science

The initial single yeast cell adhesion on glass via optical trapping and Derjaguin-Landau-Verwey-Overbeek predictions

Mickaël Castelain, F. Pignon, J. M. Piau, A. Magnin

► **To cite this version:**

Mickaël Castelain, F. Pignon, J. M. Piau, A. Magnin. The initial single yeast cell adhesion on glass via optical trapping and Derjaguin-Landau-Verwey-Overbeek predictions. *Journal of Chemical Physics*, 2008, 128 (13), pp.135101. 10.1063/1.2842078 . hal-02658357

HAL Id: hal-02658357

<https://hal.inrae.fr/hal-02658357>

Submitted on 13 Jan 2022

HAL is a multi-disciplinary open access archive for the deposit and dissemination of scientific research documents, whether they are published or not. The documents may come from teaching and research institutions in France or abroad, or from public or private research centers.

L'archive ouverte pluridisciplinaire **HAL**, est destinée au dépôt et à la diffusion de documents scientifiques de niveau recherche, publiés ou non, émanant des établissements d'enseignement et de recherche français ou étrangers, des laboratoires publics ou privés.

The initial single yeast cell adhesion on glass via optical trapping and Derjaguin–Landau–Verwey–Overbeek predictions

Mickaël Castelain,^{a)} Frédéric Pignon,^{b)} Jean-Michel Piau, and Albert Magnin
Laboratoire de Rhéologie, Université Joseph Fourier Grenoble I, Institut National Polytechnique de Grenoble, CNRS, UMR 5520, B.P. 53, F-38041 Grenoble Cedex 9, France

(Received 1 August 2007; accepted 17 January 2008; published online 1 April 2008)

We used an optical tweezer to investigate the adhesion of yeast *Saccharomyces cerevisiae* onto a glass substrate at the initial contact. Micromanipulation of free-living objects with single-beam gradient optical trap enabled to highlight mechanisms involved in this initial contact. As a function of the ionic strength and with a displacement parallel to the glass surface, the yeast adheres following different successive ways: (i) Slipping and rolling at 1.5 mM NaCl, (ii) slipping, rolling, and sticking at 15 mM NaCl, and (iii) only sticking at 150 mM. These observations were numerous and reproducible. A kinetic evolution of these adhesion phenomena during yeast movement was clearly established. The nature, range, and relative intensity of forces involved in these different adhesion mechanisms have been worked out as a quantitative analysis from Derjaguin–Landau–Verwey–Overbeek (DLVO) and extended DLVO theories. Calculations show that the adhesion mechanisms observed and their affinity with ionic strength were mainly governed by the Lifshitz–van der Waals interaction forces and the electrical double-layer repulsion to which are added specific contact forces linked to “sticky” glycoprotein secretion, considered to be the main forces capable of overcoming the short-range Lewis acid-base repulsions. © 2008 American Institute of Physics.
 [DOI: 10.1063/1.2842078]

I. INTRODUCTION

Micro-organisms are ubiquitous in both natural and industrial environments. They are typically tethered to surfaces as individual cells or as part of a biofilm.¹ They are beneficial, for instance, to degrade environmental hazardous substances in the soil as biofiltration but also detrimental such as on agroindustry, on ship hulls, on biomaterial implants, or in the oral cavity.^{2–4}

The yeast cell *Saccharomyces cerevisiae* was selected for this research.^{5–7} This system is widespread in agroindustry and is regarded as the model for studying the eukaryotes because of its entirely sequenced genome and its ability to initiate a biofilm.⁹ The cell wall of yeast is the only interface of the adhesion phenomenon and plays a crucial role in the process. The cell wall is 100–200 nm thick¹⁰ and envelopes the whole cell. Its rigidity¹¹ and its unique macromolecular organization give the yeast a specific shape. Two transport and secretion processes may be deeply involved in adhesion. Indeed, owing to its selective-permeability wall, the yeasts control the concentration of solutes inside the cell and so control intracellular osmotic pressure.¹² Moreover, ionic transfer between the yeasts and the extracellular medium via channels is now well understood.^{6,10,13}

To probe the relevant scales affecting the mechanisms of yeast adhesion, an optical tweezer device was set up. The time-dependent mechanisms on glass substrates were ob-

served and interpreted in terms of interaction forces of the yeast/glass system and through Derjaguin–Landau–Verwey–Overbeek (DLVO) and extended DLVO (XDLVO) calculations.

Long-range surface forces play a major role during the microbial transport process. Indeed, the adhesion process is regarded as being governed by physical and/or chemical interactions between the micro-organism and the substrate.¹⁴ Various works have investigated the adhesion of micro-organisms on inert surfaces probed by an optical tweezer^{15,16} or atomic force microscopy (AFM).¹⁷ For instance, Bowen *et al.*¹⁷ used AFM to study the adhesion of *S. cerevisiae* yeast on hydrophilic mica surfaces coated with a hydrophobic material. A single yeast cell was grafted on the cantilever tip, which was brought into contact with the surface. These authors demonstrated that the contact time was of primary importance in the adhesion phenomenon. Klein *et al.*¹⁸ used a single-beam gradient optical trap to micromanipulate a spherical bacterium against a flat glass surface. They worked out forces ranging from 0.01 to 4 pN and determined DLVO profiles as a function of the separation distance. In aqueous environments, Lifshitz–van der Waals (LW) and electrostatic (EL) forces are frequent dominating factors, as described in the DLVO theory.¹⁹ Because bacteria and most synthetic and natural surfaces are negatively charged at ambient pH values, the electrostatic interaction is, as a rule, repulsive. At low ionic strength (≥ 1 mM), the long-range DLVO-type electrostatic repulsion dominates over the van der Waals attraction, but at high ionic strength, the van der Waals attraction dominates.^{19–21} However, it has been marginally successful in explaining microbial adhesion phenomena onto

^{a)}Present address: Department of Physics, Umeå University, SE-901 87 Umeå, Sweden.

^{b)}Author to whom correspondence should be addressed. Electronic mail: pignon@ujf-grenoble.fr.

various surfaces, as it does not consider non-DLVO interactions, such as hydrophobicity and hydrophilicity as described by the extended DLVO theory.^{22–28}

Israelachvili²⁹ presented the adhesion as a biospecific and nonequilibrium interaction in biological systems. He showed that biological interactions are better thought of as processes that evolve in space and time, and under physiological conditions, involved in continuous input of energy. He illustrated it with leucocytes rolling along the endothelium *in vitro* relating sticking, rolling, or slipping regarding the flow transport velocity. The author considered that each rolling involves many mobile molecules mediating a specific adhesion manner. Bathia *et al.*³⁰ found that yeast promotes specific molecules to adhere by rolling under a channel flow. Moreover, various works^{9,31,32} highlighted that protein secretion (adhesins, flocculins) toward the outer layer of the fungal cell wall³³ allows yeasts to adjust to environmental variations. Such glycoprotein, linking the cell wall to any other elements, may play a crucial role in adhesion mechanisms on a substrate.

From our local approach with an optical tweezer combined with the calculation of interaction forces, the results presented in this paper will show that the yeast adheres as ionic-strength-dependent mechanisms. Indeed, at 1.5 mM NaCl, when the cell is brought into contact by the optical trap and then moved parallel to the substrate, the yeast exhibited a singular slipping behavior, rolled for a time, and then slipped again. At 15 mM NaCl, the cell slipped as previously, rolled, and stuck to the substrate. Finally, at 150 mM NaCl, the cell completely stuck to the substrate. When yeasts tethered to the surface, the maximum forces exerted by the trap (20–30 pN) was not able to remove cells. The observations were reproducible and numerous. Few examples will be depicted. This stick-slip phenomenon is widely described by adhesion mechanisms of leukocytes where bonds between adhesion molecules are often mechanically stressed such as the tensile force applied to selectin-ligand bonds, which mediate the tethering and rolling of flowing leukocytes on vascular surfaces.³⁴

In Sec. II, we present the yeast *S. cerevisiae*, glass substrates, optical tweezer, and suitable methods for observing adhesion at the initial contact. In Sec. III, the results regarding prediction models are discussed. Additional information is given in Appendixes A and B, where a short review on electrophoretic measurement of glass and DLVO and XDLVO models, are presented, respectively.

II. MATERIALS AND METHODS

A. Yeast cells

Dried baker yeast *S. cerevisiae* has been provided by Lesaffre (Marcq-en-Baroeul, France). The material was initially packaged as dry aggregates of small rod shape. The physicochemical properties of the surface have been given in a previous work⁷ (see Table I).

1. Rehydrated yeast cells: Preparation

Yeast cells were rehydrated in saline solutions (NaCl) with 0.2 μm filtered and demineralized water (Milli-Q, Mil-

TABLE I. Zeta potential and cell wall contents of yeast cells.

	Ionic strength (mM NaCl)		
	1.5	15	150
Rehydrated yeasts			
μ (10^{-8} m ² /V/s) ^a	–2.0		–0.8
ζ (mV) ^b	-25.9 ± 1.3		-10.4 ± 1.3
Mass of the cell wall (% dry weight) ^c	Polysaccharide content of the cell wall ($\mu\text{g}/\text{mg}$ dry mass)		
	Chitin	β -glucan	Mannan
	25.8	2.14 ± 0.12	189.3 ± 7.2
			66.5 ± 1.8

^aElectrophoretic mobility, data from Ref. 7.

^b ζ potential calculated from the von Smoluchowski equation (Ref. 22).

^cSee Ref. 8.

lipore, Billerica, MA). Three NaCl ionic strengths were tested: 1.5, 15, and 150 mM. The suspension has been prepared by dispersing and rehydrating 1 g/l aggregates in the saline solution at room temperature (23 °C), with gentle agitation for 20 min. Yeast cells were harvested by centrifugation for 2 min at 15 000 rpm (Biofuge Stratos, Heraeus Instruments, Osterode, Germany), washed twice, and suspended again in NaCl solution. The pH was 5.7 at $T = (25.0 \pm 0.1)$ °C.

2. Contact angle measurement and surface tension components

Yeast cells were rehydrated and washed with pure Milli-Q water as described above. A 10-ml volume was filtered on 0.45 μm (Sartorius, Goettingen, Germany) and then dried under a vertical flow hood (Faster BH-2004, Ferrara, Italy) at room temperature (23 °C) for a specific period to obtain the so-called plateau contact angle,^{23,27} with water on lawns of partially dried yeasts using the sessile drop technique. The mentioned contact angle was obtained after 80 ± 11 min of drying (± 11 is the standard deviation of ten assays). Once the plateau contact angle reached out, three liquid probes [Milli-Q water, glycerol (Selectipur, Merck, Darmstadt, Germany), and di-iodomethane (Sigma-Aldrich and Co., Saint Louis, MO)] were deposited on lawns and angles were determined by the sessile drop technique with a goniometer (Digidrop, GBX Scientific instruments, Romans, France) at room temperature (23 °C). Results presented here are an average of ten measurements. The contact angles were then converted into surface free energy values using the modifications of Young's equation proposed by van Oss,²² which ignore spreading pressure and distinguish Lifshitz-van der Waals (LW) and Lewis acid/base (AB) free surface energy components [Eq. (B1)].

B. Optical tweezer

The setup is capable of trapping micron-sized objects with index of refraction different from those of the suspending medium. Such system, inspired by Fällman and Axner,³⁵ has been previously developed and described by Piau.³⁶ A short description will be given below following the diagram shown in Fig. 1(a), as this will be useful for this study.

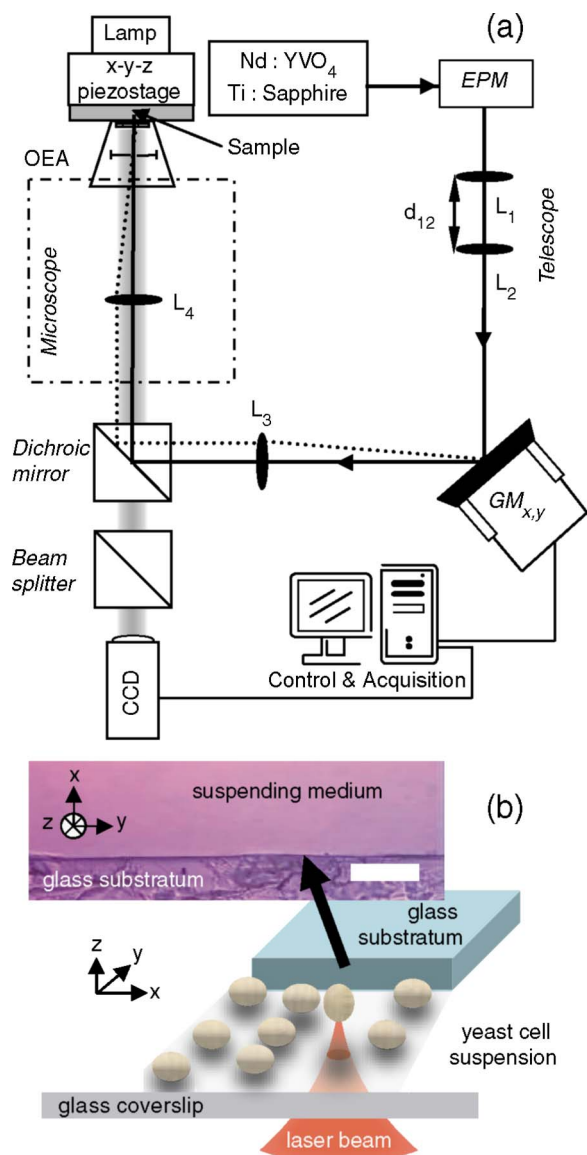


FIG. 1. (Color online) (a) Schematic layout of the optical tweezer. (b) Schematic describing the sample setup. It is composed of a glass fragment where the surface is positioned vertically and so seen in the profile (photo) and a yeast suspension of rehydrated yeast in different saline solutions. The laser beam crosses the coverslip and traps a yeast cell. Note that the schematic is not to scale. The scale bar indicates $20 \mu\text{m}$. This scheme is from previous works (Ref. 5).

The laser (Millennia V, Spectraphysics, Mountain View, CA) emitted a 532 nm beam of up to 5 W power. The wavelength of this beam is then adjusted to 800 nm, considered to be the minimum absorption level of the suspending medium⁵ by means of a Ti-sapphire (3900S, Spectraphysics, Mountain View, CA). The beam is magnified by the telescopic system consisting of two lenses (L_1 and L_2) and then directed into the galvanometric system which consists of two perpendicular mobile mirrors. Then, the beam is sent into the microscope and is focused on the sample through the objective. The distance d_{12} between the two lenses L_1 and L_2 modifies the vertical position (z) of the optical trap in the sample.

The optical tweezer was built around an inverted light microscope (Olympus IX70; Olympus, Melville, NY). Micron-sized particles require the use of a high magnifica-

TABLE II. Contact angles (deg), surface tension components (mJ/m^2), and glass surface roughness (Ref. 7).

Contact angles (deg)		
θ_{water}	$\theta_{\text{di-iodomethane}}$	$\theta_{\text{formamide}}$
32.5 ± 2.7	39.5 ± 1.7	18.1 ± 1.4
Surface energy (mJ/m^2)		
γ_S^{pdW}	γ_S^+	γ_S^-
39.9 ± 0.8	1.5 ± 0.4	38.7 ± 3.6
Roughness R_a (nm)		0.4

tion objective ($\times 100$) and a large numerical aperture increases beam stability. Thus, an oil immersion objective is used with a numerical aperture of 1.4. The refractive index of the oil used is 1.52. The display system consisted of a three charge coupled device video camera (JVC KYF55B; JVC UK Ltd, London, UK) of 25 images per second, of 768×494 pixels.

C. Solid glass substrate

A glass fragment was positioned vertically between the microscope slide and the coverslip. This slice of glass comes from an ordinary soda-lime glass plate (Planilux, Saint-Gobain, France) whose energy properties obtained by the contact angle measurement method were given in previous works⁷ (see Table II).

A made-to-order fragment was shaped from this glass plate ($210 \times 90 \times 4 \text{ mm}^3$) using the lithopreparation method (abrasion on each side) to obtain a slice 10 mm long, 4 mm wide, and $250 \pm 3 \mu\text{m}$ thick. The area where adhesion occurred was then perpendicular to the slide/coverslip system and of similar nature [energy properties and average roughness (0.25 nm)] to the top face of the original plate [see Fig. 1(b)]. Cleaning was carried out with the sulfochromic mixture for 1 h.

D. Scanning electron microscopy and x microanalysis

To determine possible damage from the machining method and cleaning with sulfochromic mixture on the final sample topography, scanning electron micrographs (JEOL JSM-6400, Jeol, Croissy sur Seine, France) and surface x microanalysis (Princeton Gamma-Tech Instruments, NJ) were carried out. Two types of samples were prepared: (i) Fragments cleaned with sulfochromic acid and (ii) fragments solely cleaned with water. The samples were air dried and metallized under vacuum before the analysis and observation.

E. Analysis chamber and protocol of measurements

Before each test, the slide, coverslip, and slice of glass were carefully cleaned with the sulfochromic mixture and dried with clean room paper. To assemble an analysis chamber, an autoadhesive frame (Geneframe 25 μl , ABgene, Epsom, UK) is fixed onto the microscope coverslip. Then the slice of glass is placed on the plate, the smooth face of the

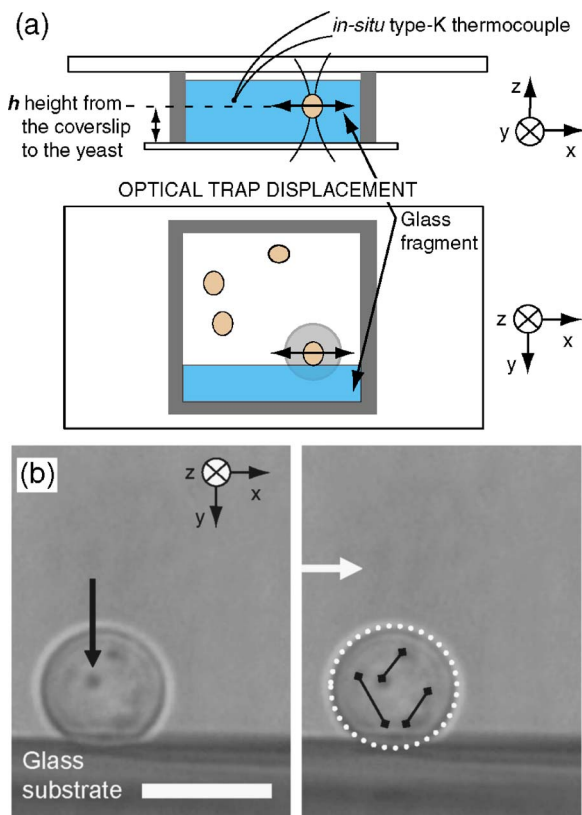


FIG. 2. (Color online) (a) Schematic of the sample seen in the profile (above) and seen from the bottom (below). During the adhesion assays, the laser moved a yeast cell along the x axis and is focused at a distance h far from the coverslip. Note that the schematic is not to scale. (b) Example of a cell in contact with the glass substrate. The two snapshots are identical. The right one is analyzed. A few fixed spots are identified within the yeast. The black arrow indicates one of these spots. The shape of the yeast is then drawn (white dotted circle). The scale bar is $5 \mu\text{m}$.

fragment in vertical plane. A volume of $25 \mu\text{l}$ of yeast suspension (about 4×10^6 cells/ml) is introduced into the chamber formed by the coverslip and the frame stuck to it. The analysis chamber is then sealed by laying the slide above, evenly stuck on the frame, while taking care to eject any air bubbles. Figure 2(a) shows the assembly. The analysis chamber is then positioned in the microscope, coverslip downward, facing the objective. A cell is trapped by the optical tweezer which enables to move it close to the substrate. Besides, the focal point positioned the cell at a vertical distance h far from the coverslip. The diameter is directly measured on the monitor and converted into micrometer. Then, it is brought in contact with the glass while taking care to focus the laser as far as the yeast radius from the coverslip to avoid exerting a vertical force on the cell. A program developed at the laboratory enables to control the galvanometric mirrors. The movement imposed on the particle is sinusoidal, parallel to the substrate along the x axis. Whatever the displacement amplitude, the movement velocity of the optical trap was fixed at $11.5 \pm 0.5 \mu\text{m/s}$ because it is estimated that this parameter is more important than the distance covered.²⁹ Two different amplitudes were applied: $10.2 \pm 0.3 \mu\text{m}$ corresponding to about two diameters and $14.0 \pm 0.3 \mu\text{m}$ corresponding to about three diameters. These two amplitudes have been applied to cover the maximum distance in the field

TABLE III. Contact angle measurement (deg) carried out on yeast lawns and surface energy components (mJ/m^2) of the rehydrated yeasts. Uncertainties are the standard deviation for all measurements.

Contact angles (deg)		
θ_{water}	$\theta_{\text{di-iodomethane}}$	$\theta_{\text{formamide}}$
34.2 ± 4.8	38.3 ± 5.6	41.1 ± 2.8
Surface energy (mJ/m^2)		
γ_S^{dW}	γ_S^+	γ_S^-
39.1 ± 1.5	0.2 ± 0.4	47.6 ± 1.6

of visualization. Indeed, glass fragments are oriented along either the x axis or y axis, but it is affirmed that the two galvanometric movements are similar and are consequently reduced to one axis by simple rotation of the picture for better observation. We will see that the amplitudes have no influence on the phenomena observed. Assays were performed at room temperature (23°C) and never exceeded 10 s.

To detect relative displacements (translation or rotation) of the yeast on the substrate, dark zones within the cell have been identified to be mainly lipid granules embedded in the cytoskeleton.^{37,38} From assumption of little movements of these reference spots, compared to the cell envelope when the yeast is trapped, the movement of the whole can be observed and so its translation or rotation can be deduced [Fig. 2(b)]. All observations confirmed that lipid granules attached to the cytoskeleton were good markers for monitoring yeast movements.

III. RESULTS

A. Surfaces properties of micro-organisms and substrates

1. Yeast cells

With Eq. (B4), tension surface components of the rehydrated yeast are reported in Table III. Rehydrated yeasts exhibited strong electron-donating and apolar components. Qualitative measurements [microbial adhesion to solvents (MATS)] were already carried out in previous works, indicating the strong hydrophilic and electron-donating components for this type of yeast.^{7,8,39}

2. Glass substrates

Scanning electron micrographs were carried out to validate the method of glass preparation (Fig. 3). Firstly, the micrographs clearly show areas which underwent abrasion because $10 \mu\text{m}$ sized fragments were torn off from the substrate. While assays were performed at $50 \mu\text{m}$ far from the edge, the effect of this rough surface did not have impact on our experiments. Since the machining is solely mechanical, this method enables to obtain a fragment on which adhesion measurements are implemented and to keep the same surface energy properties of the origin plate as well.⁷ Furthermore, cleaning with sulfochromic acid did not modify the final topography of the substrate as well. Indeed, as seen on the micrographs, Fig. 3 suggests that the roughness is less than

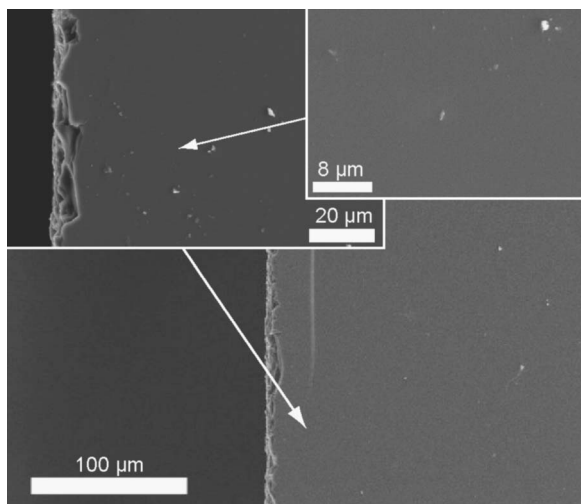


FIG. 3. Scanning electron micrographs at different magnifications of a glass fragment after machining and cleaning with sulfochromic acid. The sample has been beforehand metallized under vacuum.

200 nm here. More precise previous studies also give evidence that the roughness remained unaffected after cleaning, ranging from 0.25 nm (Ref. 40) to 0.4 nm,⁷ helped by AFM and optical three dimensional profilometry, respectively.

Finally, x-ray microanalysis determining the chemical composition of the sample provided the major presence of silicon, calcium, and sodium as described by the manufacturer for the substrates cleaned or not with sulfochromic acid.

B. Observation of the yeast/glass adhesion mechanisms

1. Slipping and rolling yeasts at 1.5 mM NaCl

Fig. 4 depicts 20 successive snapshots that are representative of our observations in the used assembly at 1.5 mM NaCl. On this illustrated example, a yeast cell of $4.90 \pm 0.05 \mu\text{m}$ diameter was brought into contact at one radius far from the surface, namely, $2.5 \mu\text{m}$. A parallel movement to the substrate was thus applied on the cell along $10.4 \mu\text{m}$ amplitude. This experiment was reproduced 38 times with different samples and with systematically different yeast cells. Laser power was fixed at 91 mW to apply a force of 20–30 pN.⁵ Two ways of displacement/adhesion were highlighted: Firstly, a single slipping mode of the yeast, namely, a translation without rotation, and secondly, a rolling mode such as a rotation and slipping of the yeast, resulting from the optical trap movement on the cell. To start with, it can be noticed that the yeast, moved by the trap, was simply translated by slipping on the glass (frames 2–10 and 15–20). This phenomenon of slipping was observed in every experiment.

Fig. 5(a) depicts snapshots resulting from the enlargement of frames 5, 6, 8, and 10 of Fig. 4. The slipping phenomenon is visible here. The circle plotted in white dotted line represents the cell at its initial position in frame 5. The black arrow indicates the center and the direction of displacement of the optical trap. The black and white alters are arbitrarily chosen spots, indicating intracellular organelles (dark zones being mainly lipid vesicles).

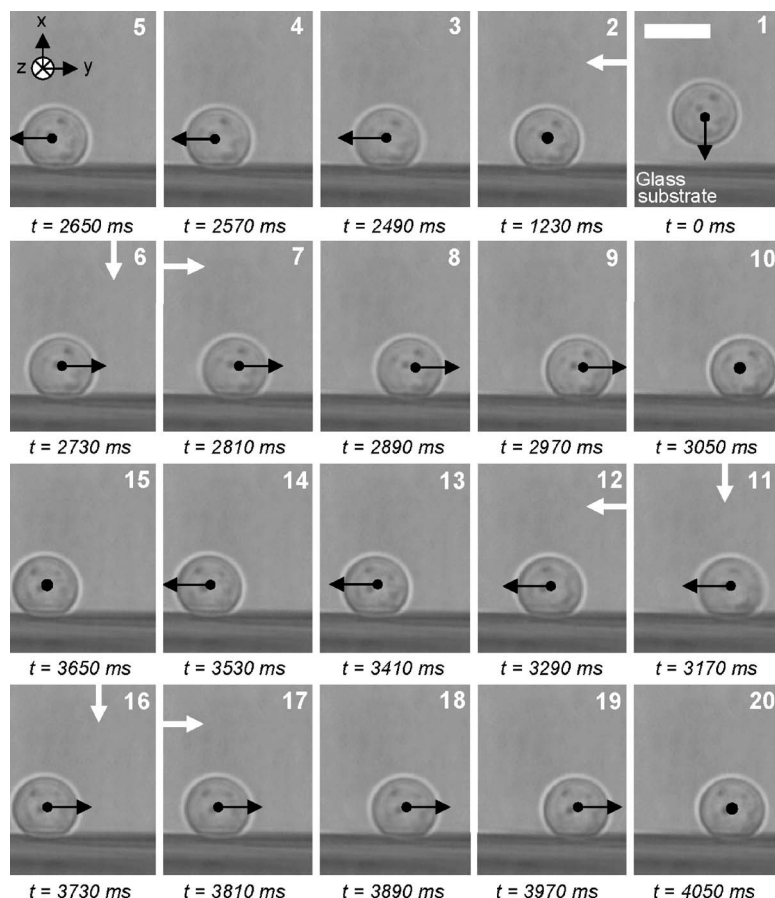


FIG. 4. Twenty successive snapshots during an adhesion experiment of yeast of $4.9 \mu\text{m}$ diameter rehydrated in a 1.5 mM NaCl solution at $d=55 \mu\text{m}$ along the z axis. The black arrow indicates the laser displacement direction. The laser power is 91 mW and the room temperature is $T=23.4 \text{ }^\circ\text{C}$. The scale bar is $5 \mu\text{m}$.

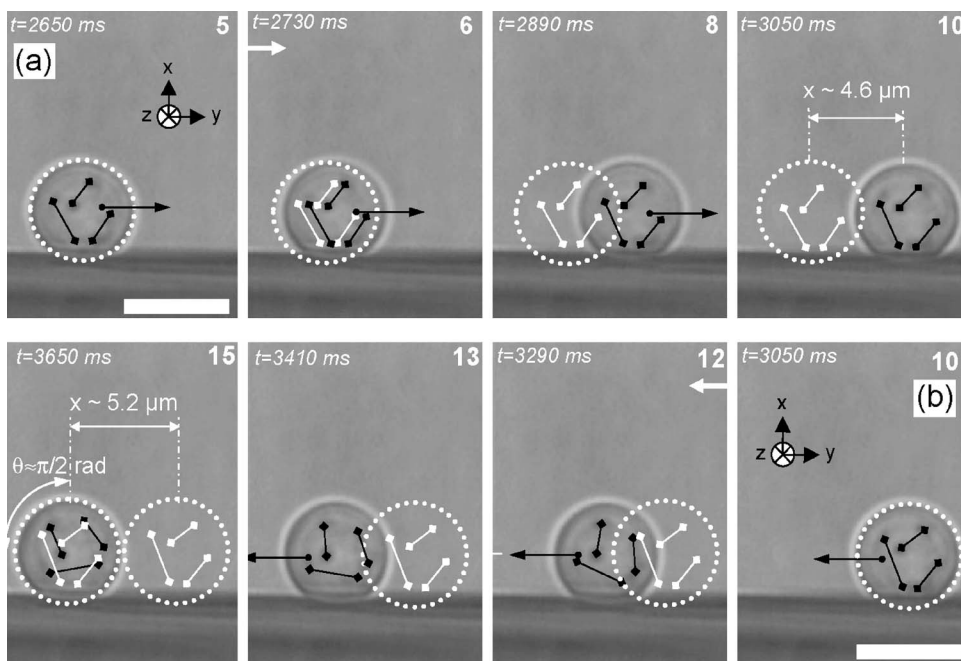


FIG. 5. Two series of four successive snapshots resulting from the enlargement of (a) frames 5, 6, 8, and 10 and (b) frames 10, 12, 13, and 15 of Fig. 4. The white marks (white alters and dotted circle) represent the yeast cell from frame 5 in (a) and frame 10 in (b) and the black arrow indicates the laser beam direction of motion. (a) Slipping effect of the yeast on the substrate at 1.5 mM NaCl. In this figure, the slipping covered distance is $4.6 \mu\text{m}$. (b) Rolling effect on the substrate at 1.5 mM NaCl. In this figure, the rolling covered distance is $5.2 \mu\text{m}$ for a rotation angle of about $\pi/2$ rad. The linear velocity is estimated to be $8.6 \mu\text{m/s}$, less than the motion velocity of the laser beam. In the case of nonslipping conditions, the distance covered should have been $3.8 \mu\text{m}$. The scale bars are $5 \mu\text{m}$.

According to Fig. 5(a), the yeast velocity is identical to the trap velocity which was $11.5 \pm 0.2 \mu\text{m/s}$. Single slipping conditions were hence confirmed. However, after a time of about 3 s, yeast stopped slipping and began to stick. The trap exerted a force momentum which led the yeast to roll. Figure 5(b) depicts enlarged snapshots of frames 10, 12, 13, and 15 from Fig. 4. Here, the yeast velocity equaled $8.6 \pm 0.2 \mu\text{m/s}$, whereas the optical trap velocity equaled $11.5 \mu\text{m/s}$. The cell was thus slowed down by sticking on glass. The angular velocity is estimated to be $2.62 \pm 0.08 \text{ rad/s}$. Nevertheless, the nonslipping conditions are not validated since the cell should have covered a distance of $3.8 \mu\text{m}$ instead of $5.8 \mu\text{m}$ in these angular velocity conditions. After having rolled, the yeast is trapped along the inverse direction and slipped again

(frames 16–20 of Fig. 4) with $11.5 \pm 0.2 \mu\text{m/s}$ in velocity. In 38 cases, 31 cases of rolling have been recorded.

2. Slipping, rolling, and sticking yeasts at 15 mM NaCl

At 15 mM, the same displacement and adhesive modes were observed. However, after a manipulation time, the yeast stuck and maximum laser power trap movement cannot remove the cell. Figures 6 and 7 represent 24 successive snapshots of a single yeast of $4.70 \pm 0.05 \mu\text{m}$ diameter. The cell was moved parallel to the surface at $11.6 \pm 0.2 \mu\text{m/s}$ and at $2.3 \mu\text{m}$ far from the substrate. In the first step, the single slipping mode was observed [Fig. 8(a)] until a time of about 3 s (frame 17 of Fig. 6) from which the yeast began to roll

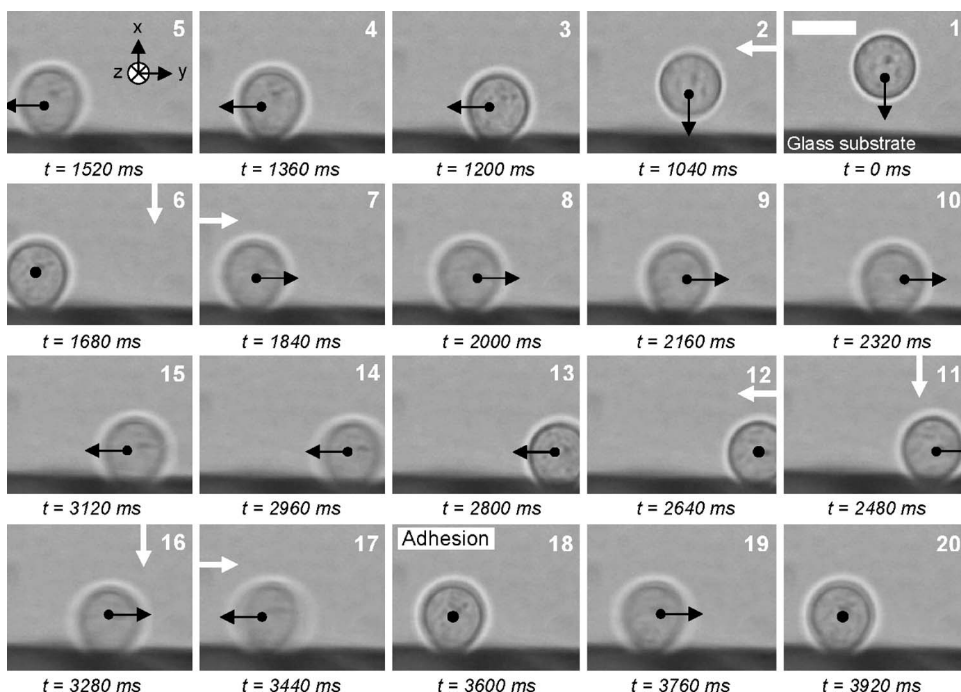


FIG. 6. Twenty consecutive snapshots during an adhesion assay of a yeast cell of $4.7 \mu\text{m}$ diameter, rehydrated in a 15 mM NaCl solution at $d=50 \mu\text{m}$ along the z axis. Frame 17 shows when the adhesion occurs. The black arrow designates the laser beam direction of motion. The laser power is 91 mW and the room temperature was measured to be $T=23.1^\circ\text{C}$. The scale bar is $5 \mu\text{m}$.

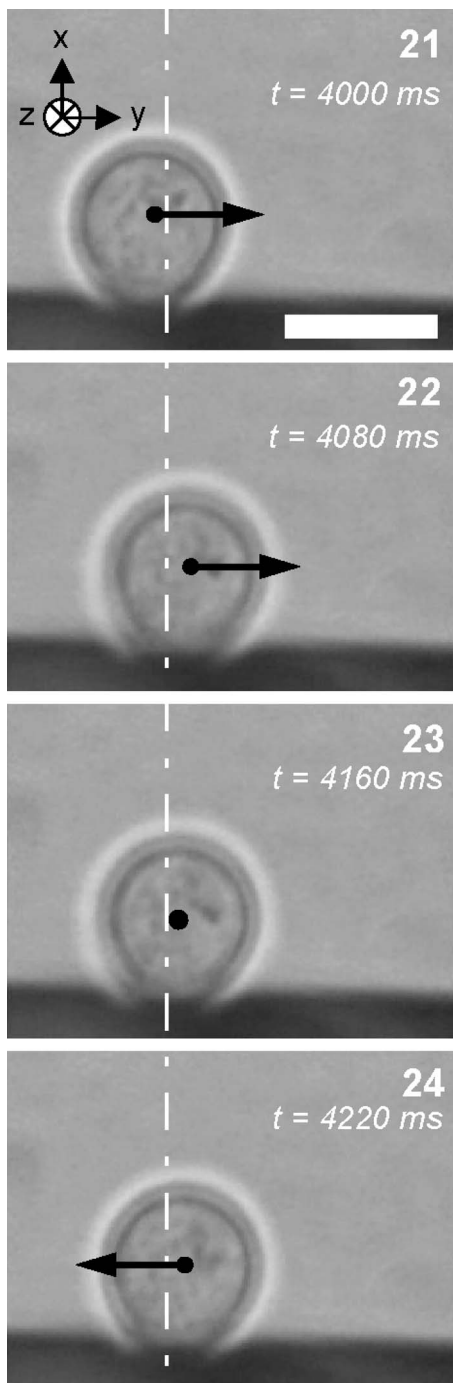


FIG. 7. Four successive snapshots following Fig. 6. The vertical white dashed line demonstrates that the adhesion is strong here in spite of the laser motion. The black arrow indicates the laser beam direction of motion. The scale bar is $5 \mu\text{m}$.

and stick [Fig. 8(b)]. This adhesion mechanism through rolling is similar to a discrete-type phenomenon, as has been highlighted previously.⁵ The glass substrate involvement (topography, surface defects) can be easily removed in this phenomenon because the cell slipped several times, successively, on the same surface (frames 5–15 of Fig. 6). At a given time, the yeast tethered to the substrate. So, the trap exerted a force momentum making the cell roll about 0.52 rad on this example presented in Fig. 8(b). Indeed, after the cell immobilization, movement of weakest amplitude

was applied but failed to remove it. The laser power was fixed at 91 mW to apply a force of 20 – 30 pN. In 27 experiments carried out, 21 experiments resulted to yeast immobilization in the same way as illustrated on this example. Furthermore, the slipping and rolling before immobilization were observed for the 27 experiments at this ionic strength.

3. Sticking yeasts at 150 mM NaCl

The yeast, of $4.80 \pm 0.05 \mu\text{m}$ diameter on this example, immediately stuck on the substrate, just after it was brought into contact. No mobility was observed when we tried to move it with the optical trap, at 91 mW in laser power corresponding to a force of 20 – 30 pN.⁵ This phenomenon was observed 42 times for each different cell. The contact time did not exceed 3 s (see Fig. 9).

These phenomena are in good agreement with previous works⁵ for which measurements and observations were performed on the rehydrated and cultured yeasts at contact times longer than 1 h and longer than those implemented in this study. Indeed, the initial contact is determinant in the following part through the DLVO and extended DLVO theories in order to identify the interactions involved in adhesion processes.

IV. DISCUSSION: DLVO AND XDLVO ANALYSES OF INTERACTIONS IN ADHESION PROCESSES

At the initial contact, it was observed that adhesion is strongly influenced by the ionic strength of the suspending medium. These results can be interpreted in terms of nonspecific interactions regarding the DLVO and extended DLVO theories (Appendix B). From the measurements of electrophoretic mobility and the contact angle on partially dried yeast lawns, the yeasts are strongly hydrophilic and negatively charged (see Table I) and exhibited a strong electron-donating component. These properties were already observed by the qualitative MATS method^{7,27,39} and also by the contact angle measurement on yeast lawns. Thus, we determine in this part profiles of energy components involved in adhesion processes. To calculate the total energy of adhesion, it is necessary to rule and know a few parameters. Otherwise, in a previous bibliographic study,⁵ it was shown that the laser beam did not damage biological trapped objects by the radiation or thermal effect. Moreover, other authors^{41,42} were interested in the metabolic activity of trapped yeasts and showed that the yeasts budded as well as the untrapped ones. Unpublished data, inspired by these works, validated these results in our own configuration of the optical tweezer (the wavelength, particularly).

A. Determination of the electrostatic component

According to Eqs. (B7) and (B10)–(B12), the EL component is determined. Here, the zeta potential measurement of the glass substrate is quite debatable (for more details, see Appendix A). According to various authors,^{19,45,48,51} the zeta potential value linearly varies. In our range of ionic strength, namely, 1.5 – 150 mM NaCl, the values extracted from the literature are -74 mV at 1.5 mM, -50 mV at 15 mM, and

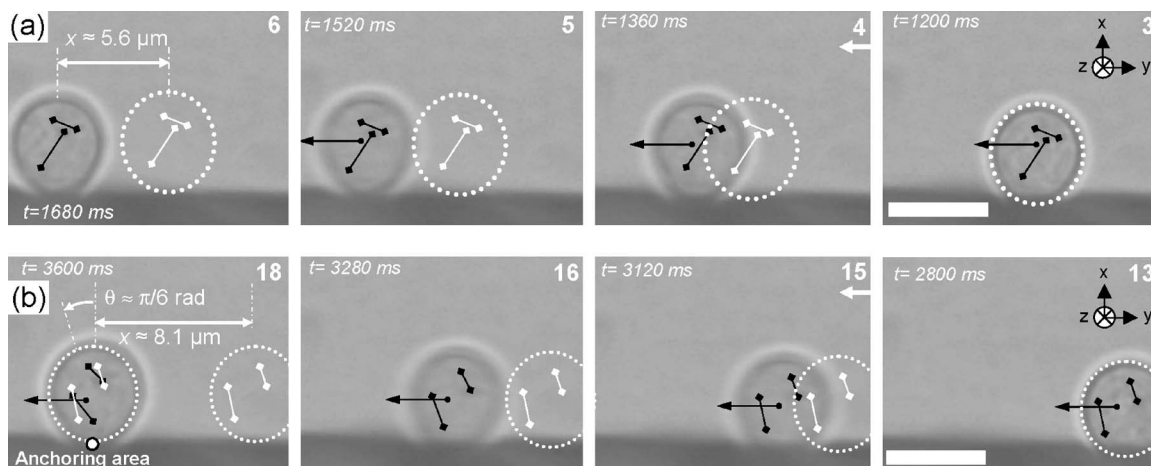


FIG. 8. Two series of four successive snapshots resulting from the enlargement of (a) frames 3–6 and (b) frames 13, 15, 16, and 18 of Fig. 6. (a) Slipping effect of the yeast cell on the substrate at 15 mM NaCl. In this figure, the slipping covered distance is $5.6 \mu\text{m}$. (b) Slipping, rolling, and sticking effect of the yeast cell on the glass substrate at 15 mM NaCl. In this figure, the slipping distance covered is $8.1 \mu\text{m}$. The rolling here is a simple rotation of $\pi/6$ rad resulting to the force momentum exerted by the trap. It is noticed that the force momentum may be created by a shear flow near a wall. The white marks (alters and dotted circle) represent the yeast at its initial position, depicted on (a) frame 3 and (b) frame 13. The black arrow indicates the laser beam direction of motion. The scale bars are $5 \mu\text{m}$.

-25 mV at 150 mM. Knowing these values, the electrostatic component can be easily plotted as a function of the separation distance [Fig. 10(a)]. The zeta potential of yeast cells was measured by Guillemot *et al.*⁷ In Table I, the values were measured at 1.5 and 150 mM. The value at 15 mM was linearly interpolated to be -18.1 mV. It is well known that, in the DLVO theory, the salt concentration increase in aqueous media leads to decrease of the surface potential of a charged surface; the electrical double layer is compressed and is thus thinned. Figure 10(a) clearly shows the decrease of the electrostatic interaction range with the ionic strength increase. Indeed, at 1.5 mM, these interactions are repulsive up to 70 nm for 1.3 kT. However, they are negative and so attractive below 0.5 nm. When the ionic strength increases, the repulsive range of this component declines down to 20 nm and 1.5 kT at 15 mM and to 5 nm and 2 kT at 150 mM. These curves demonstrate that the Debye length,

screening naturally a charged surface in a polar solvent, mainly depends on the electrolyte concentration in aqueous media in contact to the surface [Eq. (B12)]. Thus, by increasing the solute amount, this length decreases. In this analysis, it can be easily understood that the increase of ionic strength leads to decrease of the surface potential and so the electrical double-layer thickness which allows the yeasts to be closer to the substrate.

B. Determination of the polar and apolar components

With Eqs. (B5), (B6), (B8), and (B9), the LW and AB free energies at the equilibrium distance ℓ_0 and the LW and AB free energies at the separation distance h were determined, knowing the surface tension components γ^{LW} and γ^{AB} of the elements involved in the adhesion process: The yeasts and glass substrate by the contact angle measurement

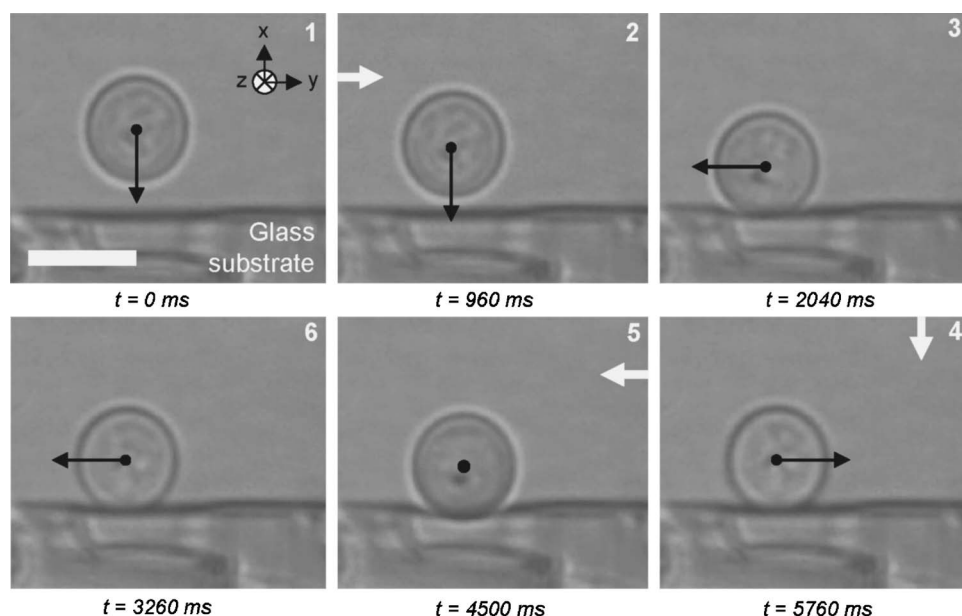


FIG. 9. Six successive snapshots during an adhesion assay of a yeast cell of $4.8 \mu\text{m}$ diameter rehydrated in a 150 mM NaCl solution at $d=60 \mu\text{m}$ along the z axis. The black arrow indicates the laser beam direction of motion. The laser power is 91 mW and the room temperature is $T=23.5^\circ\text{C}$. The scale bar is $5 \mu\text{m}$.

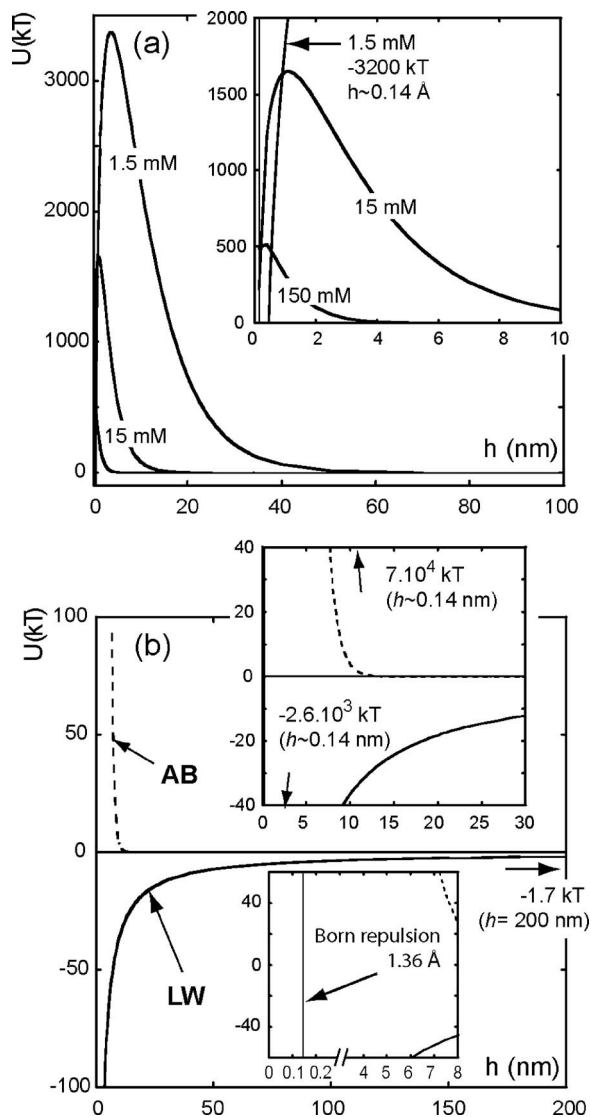


FIG. 10. (a) Electrostatic component EL (kT) and (b) apolar LW and polar AB components (kT) of the yeast/glass system as a function of the separation distance (nm) at different ionic strengths (1.5, 15, and 150 mM).

[Eq. (B4)] and water as the suspending medium to which components are already known.^{22,43,53} These calculated energies are independent of the ionic strength and can be thus plotted as depicted in Fig. 10(b). The yeasts and glass substrates are hydrophilic and their basic components are strong^{7,8,39} (Tables II and III). The hydrophilic repulsions are so dominating. Indeed, at the equilibrium distance ℓ_0 , the AB component equals 7×10^4 kT, against -2.6×10^3 kT for the LW attractive component. However, AB interactions are short-range interactions^{22,24,53} since there is no influence beyond 10 nm. These range values were cited by a few authors for different micro-organisms both exhibiting the same polar components.²⁴ The LW component is weaker than the polar component at the short range but can be extended up to 200 nm in our study where it still equals -1.7 kT [Fig. 10(b)].

C. DLVO and XDLVO profiles

The interactions involved in the adhesion mechanisms between the yeasts and glass substrate are composed of the

electrostatic repulsion, LW apolar attraction, AB polar repulsion, and physical specific interactions through “sticky” protein. All of these interactions listed can play a role in our observation analysis. To evaluate the relative importance of these different forces, energy interaction calculations from the DLVO and XDLVO models were carried out. The total interaction energy is the sum of LW and EL interactions for the DLVO interactions and the sum of LW, EL, and AB for the XDLVO interactions with Eqs. (B1) and (B11). The Brownian interaction is considered to be insignificant. Indeed, the yeast velocity on the glass is constant and the trapping laser power is high enough to ignore the thermal motion⁵ [Figs. 5(a) and 8(a)]. The sum of LW and EL interactions is reported in Fig. 11 versus the separation distance h at each ionic strength. The curves have a common tendency: The total energy passes through a first minimum and then a second minimum [Fig. 11(b)]. The DLVO interactions are essentially governed by the electrostatic repulsions at low electrolyte concentration. At 1.5 mM, the energy maximum, of the order of 3500 kT, is situated around 4 nm and is extended up to 50 nm. Beyond, the energy becomes attractive, up to 200 nm and passes through a minimum of -4.2 kT at 80 nm.

When the ionic strength increases up to 15 mM, the energy barrier decreases and comes closer to the surface, equaling 1300 kT at 1.4 nm far from the surface. The interaction is attractive from 13 nm with a minimum of -17 kT at 20 nm to about 200 nm. The energy barrier is high at the first nanometers and can explain the slipping effect of the yeasts on the substrate, mainly due to repulsion forces of this barrier. In the same way, this result of nonadhesion has already been observed in a previous work⁵ with cultured yeast cells at 1.5 mM and 1 h contact time. Nevertheless, at weak ionic strength (1.5 mM), the energy barrier seems to be too high to observe the beginning of adhesion, as shown in Figs. 4 and 5(b) by the rolling phenomenon. Among assumptions which are debated in the previous section, the discrete adhesion phenomenon may be explained by a heterogeneous zeta potential along the yeast surface. Indeed, the yeasts are provided with ion channels allowing solute transport and notably Ca^{2+} .^{6,10,13} Divalent cation in the suspending medium can have considerable effect. By adding 3 mM of calcium in a 100 mM NaCl solution, the local counterion concentration of a negative-charged surface equals $5M$ of Na^+ and $7M$ of Ca^{2+} . It is admitted that yeasts exchange this divalent cation outward.^{6,10,13} However, Ahimou *et al.*⁴⁴ concluded that the electrostatic surface distribution is heterogeneous for pH less than 6, corresponding to this study. Considering their results and AFM accuracy, this conclusion is carefully written but can be discussed at the nanometer length scales. This eventual surface potential variation may affect the electrostatic repulsions which dominate at 1.5 mM [Fig. 11(b)].

At 150 mM, the energy maximum remains negative for -48 kT and is situated at 1.1 nm. In this case, whatever the separation distance, the total interaction is attractive. This is in good agreement with our observations since the immobilization is immediate when the contact is done.

The non-DLVO component is widely taken into account in the literature^{22,25–27,53,55,57} to describe microbial adhesion.

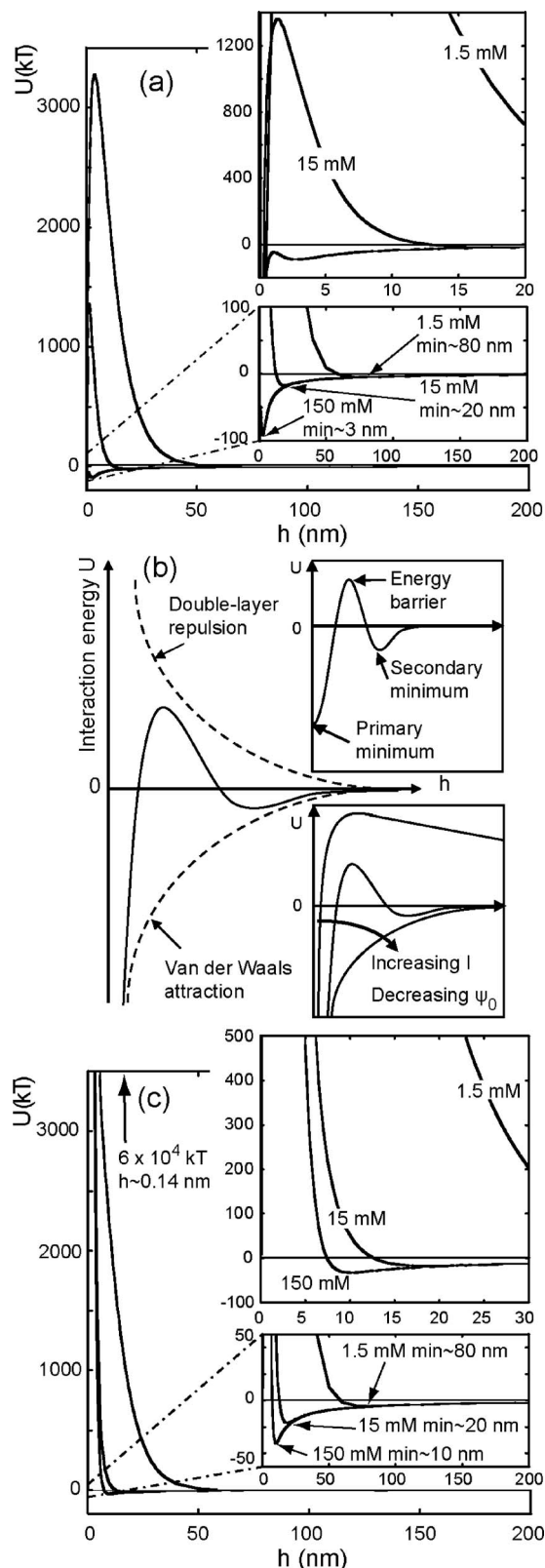


FIG. 11. (a) DLVO energy balance (kT) of the yeast/glass system as a function of the separation distance (nm) at different ionic strengths (1.5, 15, and 150 mM). (b) Classical DLVO energy balance (kT) as a function of the separation distance (nm) illustrating the first and second minima and the energy barrier. The salt concentration influences the electrostatic repulsions and so the total interaction. This example can be implemented in our results. Modified and reprinted from Ref. 58. Copyright 2007 with permission from Elsevier and Professor Jacob Israelachvili (Ref. 19). (c) XDLVO energy balance (kT) of the yeast/glass system as a function of the separation distance h (nm) at different ionic strengths (1.5, 15, and 150 mM).

This polar component considers the surface hydrophobicity which seems to be a predominant factor. In this work, polar interactions are hydrophilic and so repulsive due to hydration pressure.^{19,22} The sum of the polar AB, apolar LW, and EL components leads to the total XDLVO energy. This energy is plotted in Fig. 11(c) as a function of the separation distance h . As it has been already shown previously [Fig. 11(a)], the AB component is strongly repulsive and short ranged of about 10 nm. The DLVO profile is thus modified since there are single minima equaling -4.2 kT at 80 nm at 1.5 mM, -17 kT at 20 nm at 15 mM, and -32.6 kT at 10 nm at 150 mM. The minimum is thus shifted from 3 to 10 nm at the highest ionic strength but remains unchanged for the other cases (15 and 150 mM). Furthermore, the XDLVO maximum is higher than the DLVO maximum since it equals to 6×10^4 kT at any ionic strength against 3×10^3 kT at the weakest ionic strength. Finally, the total energy remains negative up to 200 nm.

1. What is the real hydration pressure effect on our observations?

In the range of 0–10 nm, the hydrophilic repulsion is a high energy barrier, whereas beyond this range, the energy balance follows a classical DLVO profile, as demonstrated above. In contrast to our results and our observations, the extended DLVO theory does not satisfy the mechanisms observed. A possible explanation agreeing with our observations could be biopolymeric extensions^{14,33} capable of overcoming the energy barrier and leading the observed anchorage.

In the XDLVO case, there is no first minimum due to the dominating hydrophilic repulsions. However, if those repulsions were playing a major role, there would not be variations in adhesion properties with the ionic strength. Consequently, we could wonder if those repulsions have a real short-range repulsion effect or if they are inhibited and even overcome by glycoproteins. This leads to another problematic: Does the ionic strength variation influence the glycoprotein secretion, shape,³³ and range?

2. How could outer cell glycoproteins influence adhesion?

It seems that the immobilization at 150 mM cannot only be explained by XDLVO because of the strong short-range polar repulsions. In the literature,^{5,7,39} different experiments have emphasized that yeast adhesion is drastically reduced once cells were cultured. It is concluded that unspecified sticky compounds, initially present in the culture medium or formed during the drying process, could dramatically alter the surface properties of rehydrated yeast since they remained strongly adsorbed to the cell surface even after the successive washings of the cell suspension before use. As a consequence, there is a kind of “glue” by which adhesion is efficient in spite of the polar repulsions. At 1.5 mM, the electrostatic repulsions made yeast cells far enough to avoid the sticky effect of this glue. Given this assumption, the presence of polysaccharides from cell lysis contents and eventual adhesion excretion could certainly overcome the polar repul-

sions. The use of rehydrated yeast cells is thus relevant with regard to the reproducibility of the results and the presence of adsorbed materials on the cell surface.

3. What supplementary parameters can describe the observed slipping/rolling/sticking mechanisms?

The slipping is observed before the rolling at weak ionic strengths (1.5 and 15 mM), and then rolling and/or sticking. This highlights a kinetic evolution of the adhesion properties during the slipping/rolling/sticking phenomena. As a consequence, the existence of a response time of the yeast is expected. Each rolling or sticking is observed after about 3 s. Is it a characteristic time taken by the yeast to adjust to the new imposed conditions? The obtained results enable the completion of another study⁵ at extended contact times (1–17 h) showing the kinetic influence on the removal force levels and on adhesion properties.

The glass substrate roughness was estimated to be very weak, i.e., less than 1 nm. Additionally, the substrate was cleaned by sulfochromic acid and the same surface has been covered a few times by the same yeast. Then, the yeast surface is not heterogeneous,¹⁷ and as the yeast is in translation at the beginning, the surface effect on the adhesion mechanisms can be ignored.

In summary, all of our observations and interaction energy calculations tend to describe that (i) the slipping/rolling/sticking mechanisms are linked to discrete interactions between the yeast cell wall and the glass substrate, (ii) the DLVO model which implements attractive Lifshitz–van der Waals and electrostatic repulsive forces agrees with the evolution with the ionic strength of the adhesion mechanisms observed, and (iii) the polar repulsive Lewis acid-base forces do not play a major role, probably hidden by glycoproteins on the cell wall, so far the main forces capable of overcoming the short-range Lewis acid-base repulsions.

V. CONCLUSION

The individual approach of adhesion by micromanipulation enabled the observation of the time-dependent mechanisms brought into play at the initial contact of yeasts onto glass. It has been observed reproducibly that with regard to the physicochemical conditions of the suspending medium, the yeast slips, rolls, and sticks on the glass surface during the optical trap movement parallel to the support. A kinetic evolution of the adhesion properties during yeast movement was clearly established. The underlying mechanisms and their evolution with time and ionic strength are determinant in the initial adhesion processing and then in the early stage of biofilm formation.

The initial contact is thus relevant with regard to the biofilm formation and the adhesion processing can be resumed into three words: Slipping, rolling, and sticking. Helped by data from the literature and calculations carried out in this article, those observations were interpreted in terms of surface free energies according to the DLVO and XDLVO theories. It was demonstrated that the introduction of the polar component, here strongly repulsive, is not enough to explain the phenomena and other processes in-

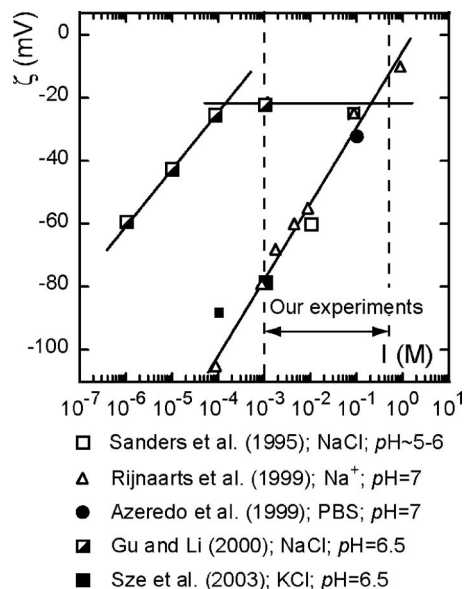


FIG. 12. Zeta potential ζ (mV) of the glass substrate as a function of the ionic strength (mM).

involved. Indeed, by the salt concentration increase, the electrical double-layer thinning shows that other attractive or adhesive effects which balance the Lewis base/base repulsions could exist. Regarding our present knowledge, we propose that adhesins or other protein anchored on the outer layer of the cell wall could be the most likely key element capable of overcoming the polar repulsions and play a dominating role on the discrete adhesion mechanism brought into light in this work.

ACKNOWLEDGMENTS

The authors are thankful to Muriel Mercier-Bonin and Philippe Schmitz for their instructive comments and for providing the biological system and glass plate. They thank Professor Jacob Israelachvili for allowing them to reprint his own figure [Fig. 11(b)] and Paul G. Rouxhet for the helpful discussions.

APPENDIX A: MICROREVIEW: ZETA-POTENTIAL OF GLASS

Various works were carried out about the electrostatic properties of the glass plate.^{19,45–52} To describe these properties, the zeta potential was determined by different authors. Figure 12 reports bibliographic data as a function of ionic strength of the suspending aqueous medium. In this graph, the zeta potential is plotted versus the ionic strength. Making the assumption that KCl and NaCl present similar electrostatic properties because they are monovalent, two types of distinct results are observed.

Firstly, whatever the solute used [NaCl, KCl, PBS (potassium buffer solution)], the zeta potential follow a linear law,^{20,45,48,51} namely, -100 mV at 10^{-4} M and -15 mV at 1 M. Indeed, Sanders *et al.*⁴⁵ analytically determined the zeta potential value by the “ionizable surface group.” The surfaces are microscope glass coverslips cleaned with sulfochromic acid, sonicated for 5 min, and stored in Milli-Q

water. Azeredo *et al.*⁴⁸ measured the zeta potential with a classical zetameter by suspending fine crushed glass particles in PBS solution. The surfaces are microscope glass coverslips cleaned with sulfochromic mixture for 24 h then with methanol and demineralized water. Sze *et al.*⁵¹ determined the zeta potential by the linear relation time-current slope of an electro-osmotic flow. The surfaces are microscope glass coverslips polished, cleaned with acetone, and air dried. Rijnaarts *et al.*²⁰ measured the zeta potential with the streaming potential of glass surfaces immersed in KCl solution. The surfaces are microscope glass coverslip stored in PBS solution.

Secondly, Gu and Li⁵⁰ determined a linear relation with the streaming potential measurement from a value of about -60 mV at $10^{-6}M$ NaCl to -20 mV at $10^{-4}M$ NaCl. Beyond $10^{-3}M$ ionic strength, the zeta values tend toward a plateau at -20 mV. The glass surfaces are microscope glass coverslips polished, stored, cleaned with acetone (12 h), stored in ultra-filtered water (12 h), and then air dried. Finally, Mala *et al.*⁴⁶ found the same results, although they are more restricted in ionic strength. A plateau of the zeta potential is obtained at -20 mV at $10^{-3}M$ KCl. These results were carried out by the stream potential measurement in a channel.

This study enables the listing of two distinct cases. The first one is a linear relation of 85 mV/M and the second one is a linear relation of 40×10^3 mV/M in slope up to $10^{-3}M$ ionic strength and beyond, a plateau at -20 mV in zeta potential. It must be underlined that the solutes, surfaces, methods of measurement, and cleaning procedures are common in both cases. However, in the first case, the authors obtained more results with varied and various methods: The stream potential measurement,²⁰ the zeta potential measurement of fine crushed glass particles,⁴⁸ theoretical and analytical methods,⁴⁵ and electrokinetic method by the time-current slope determination in an electro-osmotic flow.⁵¹ The cleaning procedures of coverslips were carried out by an acid.^{45,48} Finally, the kind of solutes does not seem to disturb the electrokinetic measurement since at a pH close to 7, the values with KNO_3 and PBS solutions are quite similar.²⁰ Those last data seem to be in better agreement with our experiments and we thus implement these values in the DLVO-type electrostatic component.

APPENDIX B: DLVO AND XDLVO THEORIES

1. DLVO and XDLVO theories

According to the DLVO theory,¹⁹ the interfacial free energies are composed of an apolar, or Lifshitz–van der Waals component, and an electrostatic component. The Brownian component will be neglected here. As suggested by van Oss,^{22,53} the extended DLVO theory in aqueous media take into account “non-DLVO” forces, namely, hydrophilic repulsion (or hydration pressure⁵⁴) and hydrophobic attraction,^{23–25,27,53} both corresponding to Lewis acid-base interactions. Thus, the interfacial free energies are composed of three components: LW, EL, and AB components. The total XDLVO energy will be described in this section. The total DLVO energy will be obtained by removing AB interactions.

The total free energy of adhesion (ΔG^{tot}) per unit area (mJ/m^2) can be written in terms of LW (ΔG^{LW}), AB (ΔG^{AB}), and EL (ΔG^{EL}),

$$\Delta G^{\text{tot}} = \Delta G^{\text{LW}} + \Delta G^{\text{EL}} + \Delta G^{\text{AB}}. \quad (\text{B1})$$

The free energy of adhesion per unit area signifies the interaction energy per unit area between two flat surfaces brought into contact with each other, which are evaluated at the equilibrium distance or closest approach ℓ_0 (according to van Oss *et al.*⁵⁵ $\ell_0 = 1.58 \pm 0.08$ Å with ± 0.08 standard deviation). We distinguish this equilibrium distance with Born repulsion equaling 1.36 Å. At the equilibrium distance ℓ_0 , where physical contact can occur,⁵⁶ $\Delta G_{\ell_0}^{\text{LW}}$ and $\Delta G_{\ell_0}^{\text{AB}}$ can be calculated using contact angle data and the acid-base approach. van Oss *et al.*⁵⁷ suggested the total surface tension of a substance to be the sum of a LW and an AB component, yielding

$$\gamma^{\text{tot}} = \gamma^{\text{LW}} + \gamma^{\text{AB}}, \quad (\text{B2})$$

where γ^{tot} is the total surface tension and γ^{LW} and γ^{AB} are the LW and AB components of the surface tension, respectively.

The AB component can be expressed as

$$\gamma^{\text{AB}} = 2\sqrt{\gamma^+ \gamma^-}, \quad (\text{B3})$$

where γ^+ and γ^- represent the electron-accepting and electron-donating parameters, respectively. The surface tension components of a solid surface (γ_s^{LW} , γ_s^- , and γ_s^+) and micro-organisms (γ_m^{LW} , γ_m^- , and γ_m^+) can be determined by measuring the contact angles using three probe liquids with known surface tension parameters (γ_l^{LW} , γ_l^- , and γ_l^+) and by implementing the extended Young equation,^{22,27,53,55}

$$(1 + \cos \theta) \gamma_l = 2(\sqrt{\gamma_s^{\text{LW}} \gamma_l^{\text{LW}}} + \sqrt{\gamma_s^+ \gamma_l^-} + \sqrt{\gamma_s^- \gamma_l^+}), \quad (\text{B4})$$

where θ is the contact angle. Expressions for the LW, AB, and EL free energies per unit area at the separation distance ℓ_0 (1.58 Å) is given by Eqs. (B5)–(B7) based on plate-plate interactions.^{22,24,53,55}

$$\Delta G_{\ell_0}^{\text{LW}} = -2(\sqrt{\gamma_s^{\text{LW}}} - \sqrt{\gamma_l^{\text{LW}}})(\sqrt{\gamma_m^{\text{LW}}} - \sqrt{\gamma_l^{\text{LW}}}), \quad (\text{B5})$$

$$\begin{aligned} \Delta G_{\ell_0}^{\text{AB}} = & 2\{(\sqrt{\gamma_m^+} - \sqrt{\gamma_l^+})(\sqrt{\gamma_m^-} - \sqrt{\gamma_l^-}) \\ & - (\sqrt{\gamma_m^+} - \sqrt{\gamma_l^+})(\sqrt{\gamma_m^-} - \sqrt{\gamma_l^-}) \\ & - (\sqrt{\gamma_s^+} - \sqrt{\gamma_l^+})(\sqrt{\gamma_s^-} - \sqrt{\gamma_l^-})\}, \end{aligned} \quad (\text{B6})$$

$$\begin{aligned} \Delta G_{\ell_0}^{\text{EL}} = & \frac{\epsilon_0 \epsilon_r \kappa}{2} (\psi_s^2 + \psi_m^2) \\ & \times \left(1 - \coth(\kappa \ell_0) + \frac{2\psi_s \psi_m}{\psi_s^2 + \psi_m^2} \text{csch}(\kappa \ell_0) \right), \end{aligned} \quad (\text{B7})$$

where ϵ_0 and ϵ_r are the dielectric permittivities of vacuum and water, respectively, κ the inverse Debye screening length, and ψ_s and ψ_m the surface potentials of the surface and cells, respectively.

Finally, the interaction energy between sphere cells and flat surfaces along the separation distance h can be calculated using Derjaguin’s approximation and written as

$$U^{LW}(h) = 2\pi\Delta G_{\ell_0}^{LW} \frac{\ell_0^2 a_p}{h}, \quad (\text{B8})$$

$$U^{AB}(h) = 2\pi a_p \lambda \Delta G_{\ell_0}^{AB} e^{-(\ell_0 - h/\lambda)}, \quad (\text{B9})$$

where λ is the decay length of AB interactions in water in the range of 0.6–1.0 nm (Refs. 19 and 22) when interactions are repulsive (hydrophilic interaction or hydration pressure). In this paper, 1.0 nm value is implemented for energy calculations,

$$U^{EL}(h) = \pi\epsilon_0\epsilon_r a_p \left[2\psi_m\psi_s \ln\left(\frac{1 + e^{-\kappa h}}{1 - e^{-\kappa h}}\right) + (\psi_m^2 + \psi_s^2) \ln(1 - e^{-2\kappa h}) \right], \quad (\text{B10})$$

where a_p is the mean radius of the yeast. $U^{LW}(h)$, $U^{AB}(h)$, and $U^{EL}(h)$ are the interaction energies of the LW, AB, and EL components at the separation distance h , respectively.

To determine the electrostatic component, it is important to know beforehand the surface potentials of the yeast ψ_m and the glass surface ψ_s [Eqs. (B7) and (B10)]. To do this, it is necessary to measure the zeta potential and deduce the surface potential ψ by using the Debye–Hückel approximation²² because it ranges from 240 to 2400 for the yeasts in this study,

$$\psi_0 = \zeta \left(1 + \frac{z}{a_p} \right) e^{\kappa z}, \quad (\text{B11})$$

where ψ_0 and ζ are the surface potentials and zeta potentials, respectively, and z is the slipping distance (0.3 nm).

The Debye screening length κ^{-1} can be easily determined with the following relation, in the case of an electrolyte 1:1 in aqueous medium:¹⁹

$$\kappa^{-1} = 0.304 \sqrt{[\text{Na}^+]}, \quad (\text{B12})$$

where $[\text{Na}^+]$ is the concentration (M) and κ^{-1} the Debye screening length (μm). The profile of the total interaction energy (ΔU^{tot}) between *S. cerevisiae* and the glass substrate can be plotted using Eq. (B13) as a function of separation distance h

$$U^{\text{tot}} = U^{LW} + U^{AB} + U^{EL}. \quad (\text{B13})$$

¹P. Watnick and R. Kolter, *J. Bacteriol.* **182**, 2675 (2000).

²J. Chandra, P. K. Mukherje, S. D. Leidich, F. F. Faddoul, L. L. Hoyer, L. J. Douglas, and M. A. Ghannoum, *J. Dent. Res.* **80**, 903 (2001).

³H. J. Busscher, R. Bos, and H. C. van der Mei, *FEMS Microbiol. Lett.* **128**, 229 (1995).

⁴H. J. Busscher, A. H. Weerkamp, H. C. van der Mei, A. W. J. van Pelt, H. P. de Jong, and J. Arends, *Appl. Environ. Microbiol.* **48**, 980 (1984).

⁵M. Castelain, F. Pignon, J.-M. Piau, A. Magnin, M. Mercier-Bonin, and P. Schmitz, *J. Chem. Phys.* **127**, 135104 (2007).

⁶R. S. Pereira, *Mol. Cell. Biochem.* **228**, 1 (2001).

⁷G. Guillemot, G. Vaca-Medina, H. Martin-Yken, A. Verhnet, P. Schmitz, and M. Mercier-Bonin, *Colloids Surf., B* **49**, 126 (2006).

⁸M. Mercier-Bonin, K. Ouazzani, P. Schmitz, and S. Lorthois, *J. Colloid Interface Sci.* **271**, 342 (2004).

⁹T. B. Reynolds and G. R. Fink, *Science* **291**, 878 (2001).

¹⁰G. M. Walker, *Yeast Physiology and Biotechnology* (Wiley, Chichester, 1998).

¹¹A. E. Smith, Z. Zhang, C. R. Thomas, K. E. Moxham, and A. P. J. Middelberg, *Proc. Natl. Acad. Sci. U.S.A.* **97**, 9871 (2000).

¹²A. J. Meikle, R. J. Reed, and G. M. Gadd, *J. Gen. Microbiol.* **134**, 3049 (1988).

¹³R. S. Pereira, *FEBS Lett.* **552**, 155 (2003).

¹⁴M. Hermansson, *Colloids Surf., B* **14**, 105 (1999).

¹⁵A. Ashkin, *Biophys. J.* **61**, 569 (1992).

¹⁶K. C. Neuman and S. M. Block, *Rev. Sci. Instrum.* **75**, 2787 (2004).

¹⁷W. R. Bowen, R. W. Lovitt, and C. J. Wright, *J. Colloid Interface Sci.* **237**, 54 (2001).

¹⁸J. D. Klein, A. R. Clapp, and R. B. Dickinson, *J. Colloid Interface Sci.* **261**, 379 (2003).

¹⁹J. N. Israelachvili, *Intermolecular and Surface Forces* (Academic, London, 1992).

²⁰H. H. M. Rijnaarts, W. Norde, J. Lyklema, and A. J. B. Zehnder, *Colloids Surf., B* **14**, 179 (1999).

²¹V. Vadiello-Rodríguez, H. J. Busscher, H. C. van der Mei, J. de Vries, and W. Norde, *Colloids Surf., B* **41**, 33 (2005).

²²C. J. van Oss, *Forces Interfaciales en Milieux Aqueux* (Masson, Paris, 1996).

²³A. M. Gallardo-Moreno, M. L. González-Martin, C. Pérez-Giraldo, J. M. Bruque, and A. C. Gómez-García, *J. Colloid Interface Sci.* **271**, 351 (2004).

²⁴J. A. Brant and A. E. Childress, *J. Membr. Sci.* **203**, 257 (2002).

²⁵K. A. Strevett and G. Chen, *Res. Microbiol.* **154**, 329 (2003).

²⁶K. W. Millsap, R. Bos, H. J. Busscher, and H. C. van der Mei, *J. Colloid Interface Sci.* **212**, 495 (1999).

²⁷S. Kang and H. Choi, *Colloids Surf., B* **46**, 70 (2005).

²⁸R. Bos and H. J. Busscher, *Colloids Surf., B* **14**, 169 (1999).

²⁹J. N. Israelachvili, *Q. Rev. Biophys.* **38**, 331 (2005).

³⁰S. K. Bathia, J. S. Swers, R. T. Camphausen, K. D. Wittrup, and D. A. Hammer, in 28th Annual Northeast Bioengineering Conference, edited by IEEE (IEEE, Philadelphia, PA, 2002).

³¹F. M. Klis, P. Mol, K. Hellingwerf, and S. Brul, *FEMS Microbiol. Rev.* **26**, 239 (2002).

³²K. J. Verstrepen, T. B. Fink, and G. R. Fink, *Nat. Rev. Microbiol.* **2**, 533 (2002).

³³K. J. Verstrepen and F. M. Klis, *Mol. Microbiol.* **60**, 5 (2006).

³⁴B. T. Marshall, M. Long, J. W. Piper, T. Yago, R. P. McEver, and C. Zhu, *Nature (London)* **423**, 190 (2003).

³⁵E. Fällman and O. Axner, *Appl. Opt.* **36**, 2107 (1997).

³⁶J.-M. Piau, *J. Non-Newtonian Fluid Mech.* **144**, 1 (2007).

³⁷I. M. Tolić-Nørrelykke, E.-L. Munteanu, G. Thon, L. Oddershede, and K. Berg-Sørensen, *Phys. Rev. Lett.* **93**, 078102 (2004).

³⁸I. M. Hagan, *J. Cell. Sci.* **111**, 1603 (1998).

³⁹H. Vergnault, M. Mercier-Bonin, and R.-M. Willemot, *Biotechnol. Prog.* **20**, 1534 (2004).

⁴⁰S. Lorthois, P. Schmitz, and E. Anglés-Cano, *J. Colloid Interface Sci.* **241**, 52 (2001).

⁴¹G. P. Singh, G. Volpe, C. M. Creely, H. Grötsch, I. M. Geli, and D. Petrov, *J. Raman Spectrosc.* **37**, 858 (2006).

⁴²G. Volpe, G. P. Singh, and D. Petrov, *Appl. Phys. Lett.* **88**, 231106 (2006).

⁴³F. M. Fowkes, *J. Adhes.* **4**, 155 (1972).

⁴⁴F. Ahimou, F. A. Denis, A. Touhami, and Y. F. Dufrêne, *Langmuir* **18**, 9937 (2002).

⁴⁵R. S. Sanders, R. S. Chow, and J. H. Masliyah, *J. Colloid Interface Sci.* **174**, 230 (1995).

⁴⁶G. M. Mala, D. Li, C. Werner, H.-J. Jacobasch, and Y. B. Ning, *Int. J. Heat Fluid Flow* **18**, 489 (1997).

⁴⁷A. E. Larsen and D. G. Grier, *Nature (London)* **385**, 230 (1997).

⁴⁸J. Azeredo, J. Visser, and R. Oliveira, *Colloids Surf., B* **14**, 141 (1999).

⁴⁹T. M. Squires and M. P. Brenner, *Phys. Rev. Lett.* **85**, 4976 (2000).

⁵⁰Y. Gu and D. Li, *J. Colloid Interface Sci.* **226**, 328 (2000).

⁵¹A. Sze, D. Erickson, L. Ren, and D. Li, *J. Colloid Interface Sci.* **261**, 402 (2003).

⁵²S. H. Berhens and D. G. Grier, *J. Chem. Phys.* **115**, 6716 (2001).

⁵³C. J. van Oss, *Colloids Surf., A* **78**, 1 (1993).

⁵⁴C. J. van Oss, *Colloids Surf., B* **54**, 2 (2007).

⁵⁵C. J. van Oss, M. K. Chaudhury, and R. J. Good, *Chem. Rev. (Washington, D.C.)* **88**, 927 (1988).

⁵⁶G. Speranza, G. Gottardi, C. Pederzoli, L. Lunelli, R. Canteri, L. Pasquardini, E. Carli, A. Lui, D. Maniglio, M. Brugnara, and M. Anderle,

Biomaterials **25**, 2029 (2004).

⁵⁷C. J. van Oss, L. Ju, M. K. Chaudhury, and R. J. Good, *J. Colloid Interface Sci.* **128**, 313 (1988).

⁵⁸J. Israelachvili, *Intermolecular and Surface Forces*, 2nd ed. (Elsevier, New York, 2007), Chap. 12, p. 248.